Radboud University Nijmegen

Faculty of Science (FNWI)

High Energy Physics

Identifying Glashow Resonance Candidates Using a Monte Carlo Simulation of Cosmogenic Neutrinos

Author:
Robin Rietman

Supervisor:
prof. dr. Ronald Kleiss

December 2020

Abstract

Cosmogenic neutrinos originate from the interaction of intergalactic ultra-high-energy cosmic rays (UHECR) with photons of the cosmic microwave background (CMB). This process is known as the GZK process, which predicts an upper limit on the energies of cosmic rays of $E_{GZK} = 5 \cdot 10^{19}$ eV. A flux of cosmogenic neutrinos is expected due to the decay of pions, which are created by the GZK process. Ultra-high-energy neutrinos are of great research interest, but currently remain undetected. The Glashow Resonance (GR) could increase the ease of detectiong of cosmogenic $\overline{\nu_e}$ at $E_{GR} = 6.3 \cdot 10^{15}$ eV. In this bachelor thesis, the feasability of measuring cosmogenic neutrinos using the Glashow resonance is researched by performing a Monte Carlo simulation, assuming mono-energetic cosmic rays with a pure proton composition. Two different decay scenarios were simulated: a two-body and a three-body decay simulation. The results show that both simulations describe the same physics, within the reached accuracy, as expected. The simulation finds that for every 100,000 GZK interactions, about 1-30 GR candidate $\overline{\nu_e}$ are expected, depending on the GR resonance range that is chosen. To conclude, further research needs to be done to determine the feasibility of using the GR in cosmogenic neutrino research and to determine what information we can extract from GR neutrino measurements.

Acknowledgements

First I would like to thank prof. Ronald Kleiss for giving me the opportunity to do my bachelor internship at the High Energy Physics department and for being my supervisor. I would also like to thank Ronald for all the thorough explanations, valuable feedback and troubleshooting with my simulation.

Secondly I would like to thank dr. Charles Timmermans for his insights and help on the cosmic ray physics related to my research.

Finally, I want to thank everybody who helped me during my bachelor thesis, both inside and outside the department.

Contents

1 Introduction **4**

2 The Greisen-Zatsepin-Kuzmin Limit **6**
2.1 Derivation of the GZK Limit 7
2.2 GZK neutrinos 9

3 Glashow Resonance **10**

4 Phase-space **13**
4.1 Two-body phase space 13
4.2 Three-body phase space 16
4.2.1 Generating $\phi_{12}, \cos(\theta_1)$ and ϕ_1 18
4.2.2 Generating energies in three-body phase space 19

5 Monte Carlo Simulation of GZK Neutrinos **21**
5.1 Generating the four-momentum of π^+ and μ^+ 21
5.2 Generating the four-momentum of $\overline{\nu_\mu}$ 22
5.2.1 Using two-particle phase-space 22
5.2.2 Using three-particle phase space 23
5.3 Boosting $\overline{\nu_\mu}$ 24
5.4 Checks 25
5.5 Selecting Glashow Resonance Candidates 25

6 Results **26**

7 Conclusion and Discussion **30**

Bibliography **32**

A Derivation of Δ^+ boost **36**

B Additional Results **36**
B.1 Two-body Decay Monte Carlo Simulation of $\overline{\nu_\mu}$ 36
B.2 Three-body Decay Monte Carlo Simulation of $\overline{\nu_\mu}$ 39
B.3 Generated Mass of W-boson 42

1 Introduction

Ever since their discovery, cosmic rays have proven to be a mystery for physicists. They can originate from a large variety of sources and differ vastly in their composition, but all cosmic rays have in common that they are particles that transverse the universe. Nowaday, most physics research focused on high-energy cosmic rays. The energies associated with cosmic rays span a spectrum of 10 orders of magnitude, with a flux spanning over 30 orders of magnitude. Particle accelerators on earth, such as the LHC, cannot even reach energies close to those of some cosmic rays. These ultra-high-energy cosmic rays (UHECR) have energies beyond 10^{18} eV. It is assumed that these UHECR have extragalactic origins, such as pulsars, gamma ray bursts and active galactic nuclei. Their precise origin still proves to be a mystery, though. Finding the sources of these highly energetic particles will give insight into what processes in the universe are able to accelerate particles to extreme energies, which could even point to beyond standard model physics [1]

Cosmic ray physics, specifically involving UHECR, thus proves to be very interesting. Unfortunately, measuring cosmic rays is hindered by several factors. Firstly, cosmic rays are deflected by cosmic magnetic fields. The cosmic rays we measure will thus rarely point straight back to their source. They can also lose energy when travelling through the universe, for example due to influence of extragalactic magnetic fields or collisions with other particles. Lastly, UHECR above a certain energy will also interact with photons of the Cosmic Microwave Background (CMB). This last difficulty actually gives us an opportunity: researching cosmic rays with neutrinos. The reactions of cosmic rays with CMB photons is known as the Greisen-Zatsepin-Kuzmin (GZK) cutoff or process. This interaction will produce pions that will decay and eventually produce neutrinos, so called GZK neutrinos or cosmogenic neutrinos. This cutoff has indeed been experimentally observed.[1] If this is indeed the GZK cutoff, a flux of cosmogenic neutrinos is guaranteed to exist. Figure 1 shows that cosmogenic neutrinos are one of the ways we can measure cosmic rays on Earth. Neutrinos are known to be quite difficult to detect. So why choose to detect cosmic rays using cosmogenic neutrinos?

The same thing that makes neutrinos difficult to measure, makes them excellent candidates to research cosmic rays. Neutrinos are weakly interacting as they are electrically neutral and have a small mass. This means they are not deflected by magnetic fields and can point back at the source of the cosmic ray. They also rarely lose energy when transversing the universe. The promising nature of neutrino astrophysics is widely recognized, with experiments such as IceCube and KM3NeT already trying to measure these neutrinos. New ambitious research is also presented, such as IceCube-Gen2 and the Giant Radio

[1] The exact cause of this cutoff has not been determined yet. The GZK effect could be an explanation, but it could also be possible that cosmic sources cannot accelerate particles to higher energies than approximately 10^{20} eV.

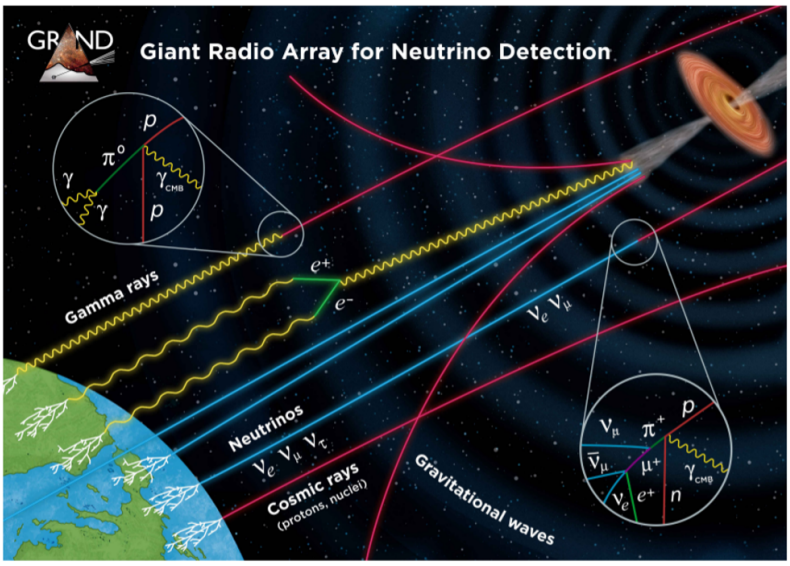

Figure 1: The propagation modes of UHECR when travelling towards earth. The GZK reactions can be seen in the circles. The π^+ is of main interest here, as this mode produces cosmogenic neutrinos. [2]

Array for Neutrino Detection, GRAND. [2, 3] These increasingly large installations all try to measure these cosmogenic neutrinos. These cosmogenic neutrinos can help us to identify the sources of cosmic rays, but they can also contribute to research on new physics such as possible neutrino decays, dark matter, hidden reactions of neutrinos with cosmic backgrounds and reactions with matter on earth.[4]

A potential method to increase the ease of detecting cosmogenic neutrinos, is the use of the Glashow resonance (GR). This is the resonant creation of a W boson by an electron and electron antineutrino. The crossection of this reaction has a strong peak at $E_{\mathrm{GR}} = 6.3$ PeV. The combination of the GZK process and the Glashow resonance should provide us with a peak in measured neutrinos at that energy, but this has not been measured yet. This brings us to the core research subject of this bachelor thesis: probing the feasability of measuring cosmogenic neutrinos using the Glashow resonance.

The goal is to determine how many GR candidates are produced by the GZK reaction. We will research this by performing a Monte Carlo simulation of the GZK process. This simulation allows us to assess the energy spectrum of cosmogenic neutrinos, which in turn can be used to determine the amount of neutrinos that are produced with energies that are relevant for GR. Before that,

the theory behind the GZK cutoff and Glashow resonance will be elaborated on in Sections 2 and 3. We will then introduce the formulas describing two-body and three-body phase space in Section 4. This information will later on be used to perform two different simulations of the GZK process. The method used to simulate the GZK process is explained in Section 5. This section will define how both descriptions of phase space are used in the simulation and cover the boosts used in the simulation. Finally, this section will give the criteria used to select a GR candidate. The results of the simulations can be found in Section 6. The thesis will end with Section 7, which serves as a conclusion of the research combined with a discussion on the current status of research.

2 The Greisen-Zatsepin-Kuzmin Limit

In 1966 two different papers indepently proposed a cutoff for cosmic rays with energies above 5 $\cdot 10^{19}$ eV.[5, 6] This limit was theoretically derived by Kenneth Greisen, Georgiy Zatsepin and Vadim Kuzmin, hence the name Greisen-Zatsepin-Kuzmin limit, or GZK limit. The argument is based on the presence on the cosmic microwave background. The CMB consists of radiation which is a remnant of the very early universe. This guarantees that there is a ubiquitous presence of low energy photons. When a UHECR above a certain energy threshold travels through the universe, it will ultimately encounter one of these CMB photons. If a UHECR above this energy limit travels a distance of more than 200 Mpc ($\approx$ 640 Mlj), it will almost always have reacted with a CMB photon. We can show this using a short calculation. First we determine the mean free path. We use n = 400 photons cm^{-3} for the CMB photon number density. For the cross section, we use σ = 200 μb = 2$\cdot 10^{-28}$ cm^{-3} for the pion creation by a CMB photon and UHE proton.[5]. This gives a mean free path λ:

$$\lambda = \frac{1}{n\sigma} \tag{1}$$

$$\lambda = 12.5 \cdot 10^{25} \text{ cm} = 4 \text{ Mpc} \tag{2}$$

We can use this to calculate the fraction of protons that survives after a given distance x for an initial density I_0.

$$I(x) = I_0 e^{-x/\lambda} \tag{3}$$

In this calculation, we set the initial intensity to $I_0 = 1$ so we can determine the fraction of the initial UHECR that remain after a certain distance. Almost all UHECR with an energy above the cutoff should lie within the so called GZK horizon, we can see that this is true for x = 200 Mpc:

$$I(x = 200\text{Mpc}) = e^{-200/4} \tag{4}$$

$$I(x = 200\text{Mpc}) = e^{-50} \tag{5}$$

This is a very small number, which indicates that there exists a GZK horizon: almost all UHECR with an energy above 5 $\cdot 10^{19}$ will have a source that

lies within a radius of 200 Mpc.

It is important to note that the original derivation of the GZK cutoff was based on theoretical arguments, but nowadays this limit has experimentally been measured, for example by the HiRes experiment.[7] The cosmic ray spectrum and this cutoff can be seen in Figure 2. At energies above the GZK limit, a steep dropoff has been observed. All particles that have energies above the GZK limit are expected to originate from relatively close sources.[8]

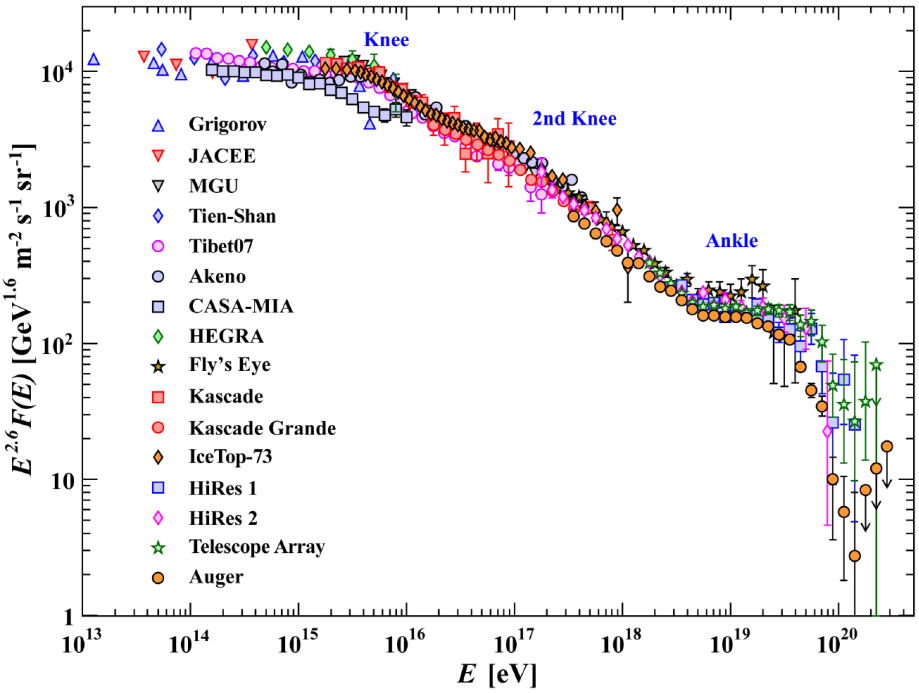

Figure 2: The measured energy spectrum of cosmic rays. The flux is plotted against the energies of the cosmic rays. After the so called 'ankle', a steep cutoff can be seen. [8]

2.1 Derivation of the GZK Limit

The GZK limit can be derived using relativistic kinematics. It is important to note that the main assumption of the derivation is that all cosmic rays consist of individual protons. This is not without issue, though. Observations of IceCube exclude pure-proton models for CR in favour of models including heavy-nuclei CR.[9] For UHECR, Auger also does not agree with this assumption, stating that the mean mass of the cosmic rays increases above enegies of about 2.5 EeV.[10] The measurements of the Telescope Array do agree with pure proton models for UHECR above the GZK limit.

In this derivation, the incoming protonic cosmic rays interact with the CMB photons through a Δ^+ resonance. This produces either a π^+ or a π^0.[2] This gives the succeeding two options:

$$\gamma_{\text{CMB}} + p \rightarrow \Delta^+ \rightarrow \begin{cases} n + \pi^+ \\ p + \pi^0 \end{cases} \tag{6}$$

In this derivation, we set c=1 and use the on-shell condition:

$$p \cdot p = m^2 \tag{7}$$
$$E^2 - |\overrightarrow{p}|^2 = m^2 \tag{8}$$

To calculate the threshold energy for the incoming proton, we want the outgoing Delta baryon to be created in it's rest system. In this derivation, the process of the photon and proton producing a Delta baryon will be used. The proton and CMB photon are assumed to be in the lab frame. We let the proton and photon collide head-on to maximise the energy made available by the collision. Both particles are set to move along the z-axis.
The momenta in the z-direction are determined using (7). Assuming that $E_p \gg m_p$, thus $E_p \approx p_p$, and using $m_\gamma = 0$ gives the following four-momenta:

$$p^\mu_{\Delta^+} = \begin{pmatrix} m_{\Delta^+} \\ 0 \\ 0 \\ 0 \end{pmatrix} \qquad p^\mu_p = \begin{pmatrix} E_p \\ 0 \\ 0 \\ E_p \end{pmatrix} \qquad p^\mu_\gamma = \begin{pmatrix} E_\gamma \\ 0 \\ 0 \\ -E_\gamma \end{pmatrix} \tag{9}$$

We can now calculate E_p by using relativistic kinematics:

$$m^2_{\Delta^+} = \left(p^\mu_p + p^\mu_\gamma\right)^2 \tag{10}$$
$$m^2_{\Delta^+} = p_p \cdot p_p + p_\gamma \cdot p_\gamma + 2p_\gamma \cdot p_p \tag{11}$$
$$m^2_{\Delta^+} = m^2_p + 0 + 2(E_p E_\gamma - (-E_p E_\gamma)) \tag{12}$$
$$m^2_{\Delta^+} = m^2_p + 4E_p E_\gamma \tag{13}$$

Rewriting to find the proton energy gives:

$$E_{\text{GZK}} = \frac{m^2_{\Delta^+} - m^2_p}{4E_{\gamma,\text{CMB}}} \tag{14}$$

[2] π^- can be produced, but this is usually suppressed.[11] Thus this will be left out here.

To compute this energy, we need the subsequent quantities and formulae:

$$
\begin{aligned}
m_{\Delta^+} &= 1232 \text{ MeV}/c^2 \\
m_p &= 938.27 \text{ MeV}/c^2 \\
T_{\text{CMB}} &= 2.726 \text{ K} \\
\lambda_{max} &= \frac{b}{T} \\
b &= 2.898 * 10^{-3} \text{ m K} \\
h &= 4.136 \cdot 10^{-15} \text{ eV s} \\
E_{\text{CMB}} &= \frac{hc}{\lambda} = \frac{hcT}{b} = 1.167 \cdot 10^{-3} \text{ eV}
\end{aligned}
$$

This gives the GZK energy threshold for the proton:

$$E_{\text{GZK}} = 1.36 \cdot 10^{20} \text{ eV} \tag{15}$$

This a higher value than the actual limit of $E_{\text{GZK}} = 5 \cdot 10^{19}$ eV. The actual CMB photons are Planck distributed in energy. The CMB photons with higher energies, in the tail of the distributions, are actually the ones that are relevant for the cutoff energy. These slightly more energetic CMB photons will interact with protons with lower energies than calculated here, explaining the difference.

2.2 GZK neutrinos

In the previous section, the energy threshold for cosmic rays protons to react with the CMB photons was calculated. This interaction creates pions which can decay into new particles. In idealised interactions, 1/3 of the cases will result in a π^+ and a neutron.[12] The pion will decay and produce neutrinos:

$$\pi^+ \rightarrow \mu^+ + \nu_\mu \tag{16}$$

$$\mu^+ \rightarrow \overline{\nu_\mu} + e^+ + \nu_e \tag{17}$$

These neutrinos are named 'cosmogenic neutrinos' or 'GZK neutrinos'. The pion decay produces neutrinos in a flavour compositon ratio $(\nu_e : \nu_\mu : \nu_\tau)$ of (1:2:0). After propagating through vacuum on cosmic scales, this distribution will change to an equal mixing of neutrino flavours because of neutrino oscillations. Thus $(\nu_e : \nu_\mu : \nu_\tau)$ will be (1:1:1) when arriving at Earth.[13] The produced neutrons can also decay further to produce neutrinos, but this process is usually suppressed and much less relevant than the pion decay.[14] GZK neutrinos are of great interest in current cosmic ray experiments, as mentioned in the introduction. The observation of the cutoff of the cosmic ray spectrum is a strong indication that there exists a cosmogenic neutrino flux.

Observations of neutrinos in the PeV and TeV range have been made by IceCube and a first possible astrophysical source of the measured neutrino has been identified.[15] Ultra-high-energy neutrinos with energies above 10^{17} have not been measured yet. These UHE neutrinos are the ones primarily associated

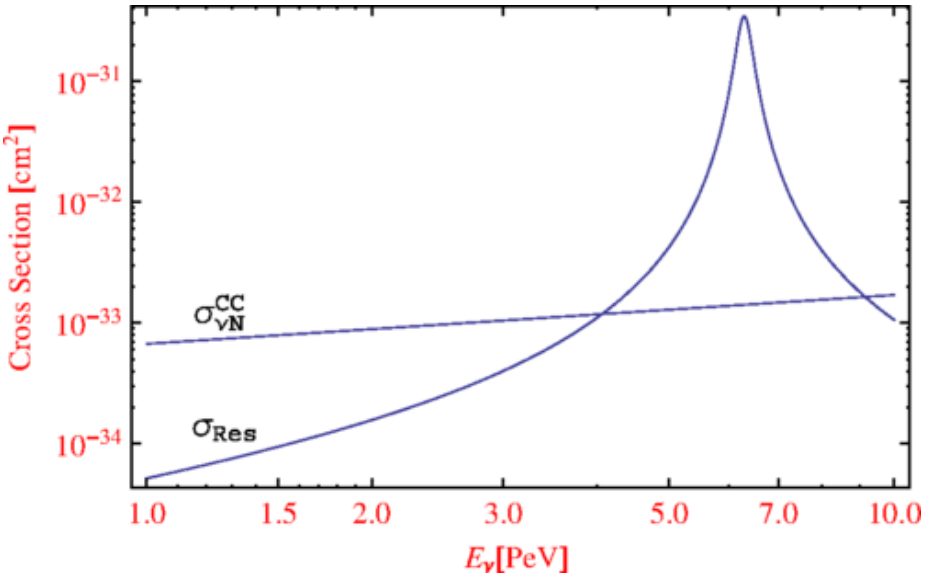

Figure 3: The Glashow resonance peak for the crossection of $\overline{\nu_e} + e^- \to W^- \to$ HADRONS compared to the crossection of $\nu_e + N \to e^- +$ HADRONS.[20]

with the GZK limit. The current absence provides an upper boundary on the flux of cosmogenic neutrinos.[16, 17] Still, the search for GZK neutrinos continues. For example with the proposed Giant Radio Array for Neutrino Detection, GRAND. This experiment aims to measure neutrinos with energies above 5 $\cdot 10^{17}$ eV using an array of thousands of radio antennas.[18]
In my research, I shall focus on the antineutrino produced by the decay of the muon. The next section will explain how these antineutrinos can be used to possibly measure cosmogenic neutrinos.

3 Glashow Resonance

The Glashow resonance was proposed by Sheldon Glashow in 1960. He describes the resonant creation of a W-boson due to the following interaction:

$$\overline{\nu_e} + e^- \to W^- \to \text{anything} \tag{18}$$

This reaction occurs at an energy of $E_{\text{GR}} \approx \frac{m^2_{\text{W}+}}{2m_e} \approx 6.3$ PeV for the incoming neutrino.[19] The crossection of the reaction of $\overline{\nu_e}$ with an electron experiences a sharp peak at 6.3 PeV, as can be seen in Figure 3. The Glashow resonance (GR) is especially interesting due to the fact that neutrinos are notoriously difficult to measure. The resonant creation of the W-boson at the Glashow resonance energy should theoretically give an excess in the measured $\overline{\nu_e}$ flux relative to other neutrinos.

To measure the Glashow resonance, one needs to have a source that can provide a flux of neutrinos with energies in the PeV range. Cosmogenic neutrinos could be good candidates to measure the GR. [21] Thus, the secondary neutrinos originating from the reaction of ultra-high-energy cosmic rays with the CMB photons might be observed by means of GR. This links the GZK limit to the Glashow resonance.

The Glashow resonance is interesting for neutrino astronomy for two reasons. Firstly, as mentioned before, the increased crossection of $\overline{\nu_e} + e^- \rightarrow W^-$ gives an enhanced measurability of cosmogenic neutrinos at $E_{GR} = 6.3$ PeV. The W-boson will then decay either into hadrons or leptons:

$$\overline{\nu_e} + e^- \rightarrow W^- \rightarrow \begin{cases} \text{HADRONS} & 68\% \\ \overline{\nu_e} + e^- & 11\% \\ \overline{\nu_\mu} + \mu^- & 11\% \\ \overline{\nu_\tau} + \tau^- & 11\% \end{cases} \tag{19}$$

These cases should provide peaks in the measurements at different energies. The hadronic decay mode accounts for 68% of the cases, which is a firm majority. This decay mode corresponds to showers with the Glashow energy of 6.3 PeV. Each lepton decay mode accounts for approximately 11% and these modes can be identified using other signals. The decay mode $W^- \rightarrow \overline{\nu_e} + e^-$ is accompanied by a peak in the energy spectrum at 3.2 PeV due to the fact that the created neutrino carries of a part of the energy.[22] The decay mode $W^- \rightarrow \overline{\nu_\mu} + \mu^-$ can be identified by a so-called 'pure muon' track. The name 'pure' originates from the fact that the only thing this mode creates inside a detector, is a muon track. The final mode $W^- \rightarrow \overline{\nu_\tau} + \tau^-$ is the 'contained lollipop'. The energy deposit is determined by the decay $\tau^- \rightarrow e^- \overline{\nu_e} \nu_\tau$, which creates a peak at an energy of 1.6 PeV. Part of the energy is carried away by neutrinos, causing the lower energy peak. This is a lower energy than the $\overline{\nu_e} + e^-$ decay mode, due to the fact that this is a three particle decay. The leptonic modes are small in the amount of events they generate, but due to their distinct signatures they could still be of importance for GR measurements.[23]

Secondly, the Glashow resonance has an important role in distinguishing how ultra-high-energy neutrinos are created. Astrophysical neutrinos can be created by either the GZK process or reactions of cosmic rays with other protons in interstellar gasses. These are also named respectively the pγ and pp processes. The pp reaction produces higher antineutrino fluxes than the pγ reaction. If more highly energetic antineutrinos are detected, pp reactions are favoured. Knowledge about the flux of high energy antineutrinos thus contributes to understanding the dominant process. The Glashow resonance is especially important here because current detectors cannot distinguish antineutrinos from neutrinos at energies above 100 TeV.[24] GR is the only process that is unique for antineutrinos and thus an important factor in measuring the neutrino to antineutrino ratio. Models where pp reactions dominate relative to pγ reactions are associated with more GR events.[25, 26] Observing this in detectors at Earth might be difficult and could require a long measurement time,

though.[12, 27] Hence, the (non-)measurement of GR can be an important probe to research the origins of astrophysical neutrinos.

Currently there has not been a conclusive measurement of a GR event. IceCube has measured some PeV neutrinos, but it is unlikely that these are GR events.[20, 28–30] The only possible candidate is a recent measurement of a cascade event with an energy of approximate 6 PeV at IceCube, which is currenty being analyzed.[15] The absence of GR events needs explanation, because a 'missing GR problem' constrains the possible models of astrophysical neutrino creation.[22] Potential options that can account for the lack of GR measurements will be discussed further on.

4 Phase-space

The objective of this bachelor thesis is to generate the energy spectrum of the neutrinos that originate from the GZK reaction to determine GR candidates. A simulation can help to describe these decay processes as we can use it to determine the four-momenta of the decay products. We can use this four-momentum to find the corresponding energy spectrum of the neutrinos. The energy spectrum can then in turn be analysed to check what fraction of particles will have an energy relevant for Glashow resonance.

Before this simulation can be done, some preliminary steps have to be made. In this section we will derive the formulas that describe two and three-body phase space. For three-particle phase space, we will derive the formulas for zero-mass particles. This is not the general description of three-body phase space, but the zero-mass case will suffice for the research done in this bachelor thesis. In particle phenomenology phase space is used to describe the final four-momenta of particles. In this case specifically, this final state will describe the four-momenta of the decay products of π^+ we want to simulate. Later the equations for two- and three-body phase space will be used to obtain two different simulations for the decays. Both simulations should describe the same physics, so both simulations will be compared to ascertain that they adhere to this principle.

4.1 Two-body phase space

First, we will discuss two-body phase space, which describes the production of two particles. An example is a decay of one particle in two new particles.

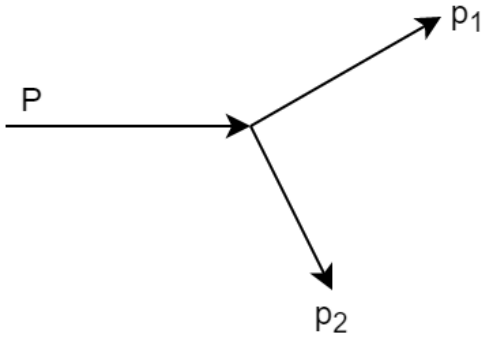

Figure 4: A sketch of the four-momenta involved in the derivation of two-body phase space. P denotes the four-momentum of the incoming particle and p_1 and p_2 denote the four-momenta of the decay products. The arrows show that P represents the ingoing particle and p_1 and p_2 represent the outgoing particles.

For a description of two-body phase space, both the integration elements over

the final four-momenta and constraints on the final four-momenta are needed. A schematic overview of the situation can be seen in Figure 4. These give the following constraints on the particles:

$$(p_1^0)^2 - |\overrightarrow{p_1}|^2 = m_1^2 \tag{20}$$
$$(p_2^0)^2 - |\overrightarrow{p_2}|^2 = m_2^2 \tag{21}$$
$$P^\mu = p_1^\mu + p_2^\mu \tag{22}$$
$$\overrightarrow{P} = \overrightarrow{p_1} + \overrightarrow{p_2} \tag{23}$$

Here P is the total four-momentum of the initial state, which is the decaying particle. p_1 and p_2 denote the four-momenta of the final states of the two particles, or the decay products in this case. (20) and (21) are the constraints imposed by the on-shell condition of the final-state particles. We recognize these formulas from Section 2.1. (22) describes the constraint on the total four-momentum due to the initial value of P, with (23) being the spatial part of the four-momentum. These constraints are combined to describe two body phase space, the delta functions refer to the restraints above:

$$dV_2(P; p_1, p_2) = d^4p_1 \delta({p_1}^2 - m_1^2) d^4p_2 \delta({p_2}^2 - m_2^2) \delta^4(P - p_1 - p_2) \tag{24}$$

These constraints denote the following delta functions in the phase space equation:

$$dV_2(P; p_1, p_2) = d^4p_1 \underbrace{\delta({p_1}^2 - m_1^2)}_{(20)} d^4p_2 \underbrace{\delta({p_2}^2 - m_2^2)}_{(21)} \underbrace{\delta^4(P - p_1 - p_2)}_{(22)} \tag{25}$$

(24) can be simplified by applying the constraints and rewriting the formula using the delta functions. This will in turn reduce the degrees of freedom and cast the phase space formula into a version that is suitable to use in a simulation: reducing the degrees of freedom increases the ease of computation. To achieve this goal, a useful convention is to choose the rest system of the incoming particle:

$$P^\mu = \left(\sqrt{s}, \overrightarrow{0}\right) \tag{26}$$

$\sqrt{s}$ denotes the invariant energy. This definition is used to impose a constraint on the final state energy, as seen below in (28). We can also cast (23) into a simpler form, which is (27):

$$\overrightarrow{p_1} + \overrightarrow{p_2} = 0 \tag{27}$$
$$p_1^0 + p_2^0 = \sqrt{s} \tag{28}$$

The following step is to rewrite the delta functions, using the constraints. Two relations for delta functions are especially important here:

$$\delta(\alpha x) = \frac{1}{\alpha}\delta(x) \tag{29}$$

$$\int_{-\infty}^{\infty} f(x)\delta(x-a)\mathrm{dx} = f(a) \tag{30}$$

(30) will often be applied without explicitly writing the integral.

Now we can write p_2 in terms of P and p_1, so we can eliminate the integration element $\mathrm{d}p_2$. The last delta function of (24) is eliminating by using (30). This allows us to define p_2 as $p_2^\mu = P^\mu - p_1^\mu$, which in turn also eliminates the integration element $\mathrm{d}p_2$ as p_2 is no longer a variable. This can be plugged into the delta function $\delta({p_2}^2 - m_2^2)$:

$$dV_2(P;p_1) \overset{(22)}{=} d^4p_1\delta({p_1}^2 - m_1^2)\underbrace{\delta((P-p_1)^2 - m_2^2)}_{(22)}$$

$$dV_2(P;p_1) \overset{(20)}{=} d^4p_1\delta({p_1}^2 - m_1^2)\delta(s + m_1^2 - m_2^2 - 2p_1^0\sqrt{s})$$

$$dV_2(P;p_1) \overset{(29)}{=} \frac{d^4p_1\delta({p_1}^2 - m_1^2)\delta(p_1^0 - \frac{s+m_1^2-m_2^2}{2\sqrt{s}})}{2\sqrt{s}}$$

In the final part of this derivation, we will recast the integral over p_1 into a simpler form:

$$\begin{aligned}
d^4p_1\delta({p_1}^2 - m_1^2) &\overset{(20)}{=} d^4p_1\delta((p_1^0)^2 - |\overrightarrow{p_1}|^2 - m_1^2) \\
&\overset{(29)}{=} \frac{d^4p_1\delta(p_1^0 - \sqrt{|\overrightarrow{p_1}|^2 - m_1^2})}{p_1^0 + \sqrt{|\overrightarrow{p_1}|^2 - m_1^2}} \\
&= \frac{dp_1^0 d^3p_1\delta(p_1^0 - \sqrt{|\overrightarrow{p_1}|^2 - m_1^2})}{p_1^0 + \sqrt{|\overrightarrow{p_1}|^2 - m_1^2}} \\
&\overset{(30)}{=} \frac{d^3p_1}{2p_1^0} \\
&= \frac{|\overrightarrow{p_1}|^2 d\cos(\theta)d\phi d|\overrightarrow{p_1}|}{2p_1^0} \\
&= \frac{|\overrightarrow{p_1}|d\cos(\theta)d\phi dp_1^0}{2}
\end{aligned}$$

In the last step we used $p_1^0 dp_1^0 = |\overrightarrow{p_1}|d|\overrightarrow{p_1}|$, which is a consequence of (20).This

result is plugged into the phase space formula, giving:

$$dV_2(P;p_1) = \frac{|\overrightarrow{p_1}|d\cos(\theta)d\phi dp_1^0\delta(p_1^0 - \frac{s+m_1^2-m_2^2}{2\sqrt{s}})}{4\sqrt{s}} \tag{31}$$

$$\overset{(30)}{=} \frac{|\overrightarrow{p_1}|d\cos(\theta)d\phi}{4\sqrt{s}} \tag{32}$$

Due to (20), $|\overrightarrow{p_1}|$ is fixed by $|\overrightarrow{p_1}| = \sqrt{p_1^0 - m_1^2}$. The delta term in (31) fixes the energy of particle one with $p_1^0 = \frac{s+m_1^2-m_2^2}{2\sqrt{s}}$. This indicates one can reduce the two-body phase space to the following proportionality:

$$dV_2(P;p_1) \propto d\cos(\theta)d\phi \tag{33}$$

Section 5 will elaborate on how this result is used in the simulation.

4.2 Three-body phase space

The process of one particle decaying into three new particles can be described using three-particle phase space. The objective is the same: determining the four-momenta of the outgoing particles. Describing this three-body case is more complicated than the two-body case, as will be seen further on. The starting point is the three particle phase space defined as following:

$$\begin{aligned} dV_3(P;p_1,p_2,p_3) = {} & d^4p_1\delta({p_1}^2 - m_1^2)d^4p_2\delta({p_2}^2 - m_2^2)d^4p_3 \\ & \cdot \delta({p_3}^2 - m_3^2)\delta^4(P - p_1 - p_2 - p_3) \end{aligned} \tag{34}$$

This formula is similar to (24), with the addition of the delta function that characterizes the constraints on the third particle. The delta functions describe similar constraints on the particles:

$$m_i^2 = (p_i^0)^2 - |\overrightarrow{p_i}|^2 \qquad i = 1,2,3 \tag{35}$$

$$P^\mu = p_1^\mu + p_2^\mu + p_3^\mu \tag{36}$$

$$\overrightarrow{P} = \overrightarrow{p_1} + \overrightarrow{p_2} + \overrightarrow{p_3} \tag{37}$$

The on-shell condition holds in the three-body case as well. The total four-momentum is denoted by P, this constrains the sum of the four-momenta of the outgoing particles. The four-momenta of the outgoing particles are denoted by p_1, p_2 and p_3. These constraints can be linked to the phase space equation as given by (34):

$$\begin{aligned} dV_3(P;p_1,p_2,p_3) = {} & d^4p_1 \underbrace{\delta({p_1}^2 - m_1^2)}_{(35),\ \mathrm{i}=1} d^4p_2 \underbrace{\delta({p_2}^2 - m_2^2)}_{(35),\ \mathrm{i}=2} \\ & d^4p_3 \underbrace{\delta({p_3}^2 - m_3^2)}_{(35),\ \mathrm{i}=3} \underbrace{\delta^4(P - p_1 - p_2 - p_3)}_{(36)} \end{aligned} \tag{38}$$

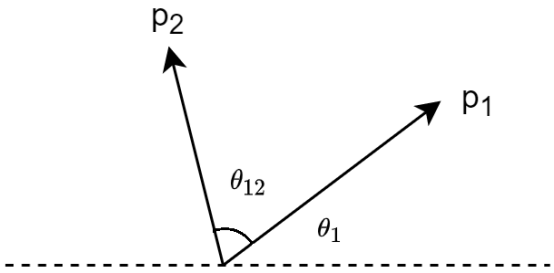

Figure 5: A two-dimensional sketch of the polar angle θ_{12} of particle 2 relative to particle 1. The polar angle of particle 1, θ_1, is defined relative to an arbitrary axis in this sketch.

Reducing the degrees of freedom of the three-body phase space is necessary to vastly increase the ease of computation when simulating the four-momenta. Thus the approach as given in section 4.1 will be used to decrease the degrees of freedom of this three-body phase space. We combine this approach with a new definition of the angles that describe the spatial components of particle 2. We name these angles ϕ_{12} and θ_{12}, which is the rotation of particle 2 with respect to particle 1. A sketch of the situation can be seen in Figure 5. Further details are explained in 4.2.1.

First, we will repeat the approach of 4.1 for the three-body phase space. We use the convention of using the rest frame of the incoming particle for the four-momentum P as given by (26). This recasts the constraint of (36) and (37):

$$\overrightarrow{p_1} + \overrightarrow{p_2} + \overrightarrow{p_3} = 0 \tag{39}$$

$$p_1^0 + p_2^0 + p_3^0 = \sqrt{s} \tag{40}$$

The constraint given by (36) can be rewritten using $p_3 = P - p_1 - p_2$. We can use this to eliminate the last delta function of (34) and the integration element dp_3. This can be combined with the result derived in 4.1:

$$d^4p_1 = \frac{|\overrightarrow{p_1}| d\Omega_1 dp_1^0}{2} \tag{41}$$

$$d^4p_2 = \frac{|\overrightarrow{p_2}| d\Omega_{12} dp_2^0}{2} \tag{42}$$

We used the definition for the solid angle: $\Omega = d\cos(\theta)d\phi$. These above results are inserted into (34). The variables $d\Omega_{12}$, θ_{12} and ϕ_{12} are introduced, which refer to the rotation of particle 2 relative to the rotation of particle 1. In the final step, we set the masses of all three outgoing particles to 0. This gives $p_{i=|\overrightarrow{p_i}|}^0$ as

per (35). We can set the masses to zero, because this is also applicable in the simulation.[3]

$$dV_3(P;p_1,p_2,p_3) = \frac{1}{4}p_1^0 p_2^0 dp_1^0 dp_2^0 d\Omega_1 d\Omega_2 \delta((P-p_1-p_2)^2 - m_3^2) \tag{43}$$

$$\overset{(35)}{=} \frac{1}{4}p_1^0 p_2^0 dp_1^0 dp_2^0 d\phi_1 d\cos(\theta_1) d\phi_{12} d\cos(\theta_{12}) \tag{44}$$
$$\cdot\, \delta(s - 2\sqrt{s}(p_1^0 + p_2^0) + m_1^2 + m_2^2 + 2p_1^0 p_2^0$$
$$- 2|\overrightarrow{p_1}||\overrightarrow{p_2}|\cos(\theta_{12}) - m_3^2)$$

$$\overset{(29)}{=} \frac{1}{8}dp_1^0 dp_2^0 d\phi_1 d\cos(\theta_1) d\phi_{12} d\cos(\theta_{12}) \tag{45}$$
$$\delta\left(\cos(\theta_{12}) - \frac{s - 2\sqrt{s}(p_1^0 + p_2^0) + 2p_1^0 p_2^0}{2p_1^0 p_2^0}\right)$$

The last result indicates that $\cos(\theta_{12})$ is set by the delta function, whereas the values for $p_1^0, p_2^0, \phi_{12}, \cos(\theta_1)$ and ϕ_1 are the remaining degrees of freedom. We cannot express these variables in terms of other variables. In the next two subsections, the generation of the energies p_1^0, p_2^0 and the angles $\phi_{12}, \cos(\theta_1)$ and ϕ_1 will be discussed.

4.2.1 Generating $\phi_{12}, \cos(\theta_1)$ and ϕ_1

As seen above, the value of $\cos(\theta_{12})$ is set by a delta function:

$$\cos(\theta_{12}) = \frac{s - 2\sqrt{s}(p_1^0 + p_2^0)}{2p_1^0 p_2^0} + 1 \tag{46}$$

The other relevant angles are variables, thus they are generated using a random number generator in a simulation. The random numbers are denoted by $\rho \in [0,1]$:

$$\phi_{12} = 2\pi\rho_1 \tag{47}$$
$$\cos(\theta_1) = -1 + 2\rho_2 \tag{48}$$
$$\phi_1 = 2\pi\rho_3 \tag{49}$$

As noted before, ϕ_{12} is the azimuthal angle with respect to the rotation of particle 1. Thus when generating the spatial elements of the four-momentum of particle 2, we need to rotate these elements with respect to particle 1.[4]. First, we define the spatial components of particle 2:

$$p_2^x = |\overrightarrow{p_2}|\sin(\theta_{12})\cos(\phi_{12}) \tag{50}$$
$$p_2^y = |\overrightarrow{p_2}|\sin(\theta_{12})\sin(\phi_{12}) \tag{51}$$
$$p_2^z = |\overrightarrow{p_2}|\cos(\theta_{12}) \tag{52}$$

[3] Three-body phase space is relevant for the decay of the muon: $\mu^+ \to \overline{\nu_\mu} + e^+ + \nu_e$. Due to the fact that $m_\mu \gg m_e, m_\nu$, it is appropriate to approximate that the masses of the decay products are zero.

[4] about this: insert picture or smth

Using the generated angles of particle 1, we rotate the spatial elements of the four-momentum of particle 2 using the following matrix multiplication:

$$\begin{pmatrix} \cos(\phi_1) & -\sin(\phi_1) & 0 \\ \sin(\phi_1) & \cos(\phi_1) & 0 \\ 0 & 0 & 1 \end{pmatrix} \begin{pmatrix} \cos(\theta_1) & 0 & \sin(\theta_1) \\ 0 & 1 & 0 \\ -\sin(\theta_1) & 0 & \cos(\theta_1) \end{pmatrix} \begin{pmatrix} p_2^x \\ p_2^y \\ p_2^z \end{pmatrix} \tag{53}$$

The rotation determines the overall spatial components of particle 2, which is compensated for the fact that the angles ϕ_{12} and θ_{12} are relative to particle 1. The spatial elements of particle 3 can then be calculated using (37).

4.2.2 Generating energies in three-body phase space

As seen above, we can write:

$$\begin{aligned} dV_3(P; p_1, p_2, p_3) =& \frac{1}{8} dp_1^0 dp_2^0 d\phi_1 d\cos(\theta_1) d\phi_{12} d\cos(\theta_{12}) \\ & \cdot \delta\left(\cos(\theta_{12}) - \frac{s - 2\sqrt{s}(p_1^0 + p_2^0) + 2p_1^0 p_2^0}{2p_1^0 p_2^0}\right) \end{aligned} \tag{54}$$

The delta function in this formula gives a constraint on the value of $\cos(\theta_{12})$, but we can also rewrite it to obtain a constraint on the values of the energies of the outgoing particles, p_1^0 and p_2^0, by using the fact that $\cos(\theta_{12}) \leq 1$.

$$\begin{aligned} \frac{s - 2\sqrt{s}(p_1^0 + p_2^0) + 2p_1^0 p_2^0}{2p_1^0 p_2^0} &\leq 1 \\ s - 2\sqrt{s}(p_1^0 + p_2^0) + 2p_1^0 p_2^0 &\leq 2p_1^0 p_2^0 \\ s - 2\sqrt{s}(p_1^0 + p_2^0) &\leq 0 \\ \frac{\sqrt{s}}{2} - (p_1^0 + p_2^0) &\leq 0 \\ p_1^0 + p_2^0 &\geq \frac{\sqrt{s}}{2} \end{aligned}$$

The last condition allows us to determine a distribution for p_1^0 and p_2^0. The condition $p_1^0 + p_2^0 \geq \frac{\sqrt{s}}{2}$ describes the upper right triangle of a plot where the x-axis is p_1^0 and the y-axis is p_2^0. This is a so called Dalitz plot, which can be seen in Figure 6.

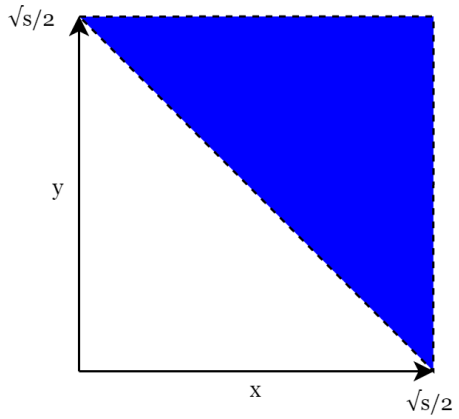

Figure 6: A schematic version of the Dalitz plot for a three particle decay where all decay products have mass zero. The x and y axes respectively correspond to p_1^0 and p_1^0. All values for x and y that fall within the blue shaded region are accepted, others are rejected.

This information can be used when generating the energies of outgoing particles 1 and 2: we can randomly generate the energies by assigning a value between 0 and $\frac{\sqrt{s}}{2}$ and then test wether it complies with the constraint given above. If it does not, the coordinates can be transformed so the energies do comply with the constraint. Here ρ also denotes a random value with $\rho \in [0, 1]$

$$p_1^0 = \frac{\sqrt{s}}{2}\rho_1 \tag{55}$$

$$p_2^0 = \frac{\sqrt{s}}{2}\rho_2 \tag{56}$$

$$p_3^0 = \sqrt{s} - p_1^0 - p_2^0 \tag{57}$$

If the demand $p_1^0 + p_2^0 \geq \frac{\sqrt{s}}{2}$ does not hold, we can transform this coordinate to make it comply with the demand:

$$p_1^0 = \frac{\sqrt{s}}{2}(1 - \rho_1) \tag{58}$$

$$p_2^0 = \frac{\sqrt{s}}{2}(1 - \rho_2) \tag{59}$$

$$\tag{60}$$

We have now derived the relevant formulas that describe three-body phase space. In the next section, we will discuss how these results are used to analyse the π^+ decay with a Monte Carlo simulation, which in turn allows us to find Glashow resonance candidates.

5 Monte Carlo Simulation of GZK Neutrinos

In this section, the method used to simulate the GZK decay process will be explained. As mentioned before, we want to simulate the energy spectrum of the $\overline{\nu_\mu}$ that is created due to the GZK process. Some of these $\overline{\nu_\mu}$ will oscillate to $\overline{\nu_e}$. These $\overline{\nu_e}$ could participate in Glashow resonance. Simulating the spectrum thus allows us to determine how many GZK neutrinos are Glashow resonance candidates.

We use a Monte Carlo simulation to achieve this goal, which is widely applied in particle physics. Monte Carlo simulation is a method which can be implemented to evaluate numerical calculations using random variables. The basis of this method is random sampling. A process is iterated many times, every time with a random input. Combining a very large amount of iterations with random numbers will give a numerical description of the simulated process. In this case, the random number generated four-momenta can be plotted into a histogram. This allows us to understand the energy spectrum of the $\overline{\nu_\mu}$ created by the GZK reaction.

The following chain of decays is simulated:

$$\Delta^+ \to \pi^+ + n \tag{61}$$

$$\pi^+ \to \mu^+ + \nu_\mu \tag{62}$$

$$\mu^+ \to \overline{\nu_\mu} + e^+ + \nu_e \tag{63}$$

The last decay is simulated using two different methods as a means to compare and check the final results. It is analyzed using either two-body or three-body phase spaced, as outlined in Section 4. Firstly, the decay process is simulated using only two-particle phase space formulas. The decay of the μ^+ is thus simulated as if the virtual W-boson created by the decaying muon is a new decaying particle. So, the W-boson is seen as an intermediate particle in the decay of the muon:

$$\begin{aligned} \mu^+ &\to \overline{\nu_\mu} + W^+ \\ W^+ &\to e^+ + \nu_e \end{aligned} \tag{64}$$

The other simulation uses the formulas of three-particle phase space to simulate the muon decay as stated in (63). It is thus the four-momentum of the $\overline{\nu_\mu}$ that is simulated in two different ways.
In this section the general procedure used in the simulation will firstly be discussed. This is followed by a description of the simulation which only uses two-particle phase spaces to describe the μ^+ decay using (64). Next, the simulation which applies three-particle phase space will be discussed. We will finally discuss how the Glashow candidates are determined.

5.1 Generating the four-momentum of π^+ and μ^+

Earlier on the framework for two-particle phase space was explained. This allows one to show that we can simulate a decay of one particle into two particles by

generating random values for the angles, ϕ and θ, of the final particles. We use spherical coordinates, where ϕ denotes the azimuthal angle and θ the polar angle. This approach is used to generate the four-momenta of π^+ and μ^+. These are used later on to generate Lorentz boosts. We will outline this for arbitrary particles *X,Y,Z*. For a general decay $X \to Y + Z$ in the restframe of X we can define the following four-momenta:

$$p_X^\mu = \begin{pmatrix} m_X \\ 0 \\ 0 \\ 0 \end{pmatrix} \quad p_Y^\mu = \begin{pmatrix} p_Y^0 \\ p_1 \sin(\phi)\cos(\theta) \\ p_1 \sin(\phi)\sin(\theta) \\ p_1 \cos(\phi) \end{pmatrix} \quad p_Z^\mu = \begin{pmatrix} p_Z^0 \\ -p_1 \sin(\phi)\cos(\theta) \\ -p_1 \sin(\phi)\sin(\theta) \\ -p_1 \cos(\phi) \end{pmatrix} \tag{65}$$

We can then define the energies of the outgoing particle and the length of the vector as following, using the derivation of two-body phase spaces as described in Section 4.1:

$$p_Y^0 = \frac{m_X^2 + m_Y^2 - m_Z^2}{2m_X} \tag{66}$$

$$p_Z^0 = \frac{m_Y^2 + m_Z^2 - m_X^2}{2m_X} \tag{67}$$

$$p_1 = \sqrt{(p_Y^0)^2 - m_Y^2} \tag{68}$$

The above parameters can be calculated using known data on the masses of the relevant particles. There are two degrees of freedom left, ϕ and θ, which are randomly generated:

$$\cos\theta = -1 + \rho_1 \tag{69}$$

$$\phi = 2\pi\rho_2 \tag{70}$$

ρ_1 and ρ_2 are two different values in the interval [0,1], generated using a uniformly distributed random number generator. Now the two different methods of generating the four-momentum of the $\overline{\nu_\mu}$ will be discussed.

5.2 Generating the four-momentum of $\overline{\nu_\mu}$

5.2.1 Using two-particle phase-space

When using two-body phase spaces to simulate the GZK process, the decay of the μ^+ is separated into two decays, as can be seen in (64). The generation of the four-momenta follows the procedure of Section 5.1, with one addition: the generation of a non-constant m_W. We do not use a set mass for the W-boson here, as the mass of the W-boson is larger than the mass of the μ^+: $m_\mathrm{W} = 80.4{\cdot}10^3$ MeV. This would cause the simulation to be physically incorrect, as a particle cannot decay into a particle with a higher mass. Thus the W-boson

decaying from a μ^+ can take on a mass between 0 and m_μ. The mass of the W-boson is generated using the contraint $\delta\left(\frac{m_\mu^2-x}{2m_\mu} - p^0_{\mathrm{W}}\right)$. The variable x denotes the variable mass as used in the simulation: $\mathrm{x} = \widetilde{m}^2_{\mathrm{W}}$, where the tilde denotes that this is the generated mass, not the W-boson mass as defined above. We can rewrite this to $\delta\left([m_\mu^2 - x] - y\right)$, with $\mathrm{y} = 2m_\mu p^0_{\mathrm{W}}$ This gives a linear distribution for x: $y = m_\mu^2 - x$. This can be simulated as stated below:

$$x = m_\mu^2 \rho_1 \tag{71}$$
$$y = m_\mu^2 \rho_2 \tag{72}$$
$$y \leq m_\mu^2 - x \tag{73}$$
$$\widetilde{m}_W = \sqrt{x} \tag{74}$$

The three-body decay has one degree of freedom more than the two-body decay. By implementing this variable W-boson mass, we introduce a new degree of freedom in the two-body decay. This variable W-boson mass restores the degree of freedom that we missed in the two-body decay simulation, giving both simulations the same amount of degrees of freedom. After generating $\widetilde{m}_{\mathrm{W}} = \sqrt{x}$ and setting $m_\nu = 0$, the four-momentum of $\overline{\nu_\mu}$ can we calculated using the procedure of Section 5.1.

5.2.2 Using three-particle phase space

In the case where we simulate the μ^+ decay as given by (63), we need to use the contraints given by three-pbody phase space. The fact that $m_\mu \gg m_{\nu_\mu}, m_{\nu_e}, m_e$ can be used to approximate that all masses of the decay products are zero. This was also used in the derivation of the formulas describing three-body phase space in Section 4.2. This allows us to use Section 4.2 for the simulation.

Referring back to Section 4.2, we can describe the energies of the particles in the three body decay by using a Dalitz plot. The Dalitz plot corresponding to this situation is an upper right triangle with $\sqrt{s} = m_\mu$, as seen in Figure 6. Only two random variables are needed, as the energy of the third particle is constrained by conservation of energy. In this case, with all decay products being massless, this gives the following distribution:

$$p^0_{\nu_e} = \frac{1}{2} m_\mu \rho_1 \tag{75}$$
$$p^0_{\nu_\mu} = \frac{1}{2} m_\mu \rho_2 \tag{76}$$
$$p^0_{\nu_e} + p^0_{\nu_\mu} \geq \frac{1}{2} m_\mu \tag{77}$$
$$p^0_e = m_\mu - p^0_{\nu_e} - p^0_{\nu_\mu} \tag{78}$$

The four-momentum for $\overline{\nu_\mu}$ can then be determined:

$$p^\mu_{\overline{\nu_\mu}} = \begin{pmatrix} p^0_{\nu_\mu} \\ p\sin(\phi)\cos(\theta) \\ p\sin(\phi)\sin(\theta) \\ p\cos(\phi) \end{pmatrix} \tag{79}$$

$$p = \sqrt{(p^0_{\nu_\mu})^2 - m^2_{\nu_\mu}} \tag{80}$$

The angles are generated as described in Section 5.1. The main difference for the four-momentum of $\overline{\nu_\mu}$ in the three-body decay case, with respect to the two-body decay case, is that $p^0_{\nu_\mu}$ is not set by constraints, but also randomly generated.

It is important to note that the simulation of the four-momenta of ν_e and e^+ deviate from this procedure. The rotation of the second decay product, ν_e, is dependent of the rotation of the first particle, $\overline{\nu_\mu}$. The four-momentum of e^+ is then defined using (36). The details can be read in Section 4.2 and will not be repeated here. It is important to generate all three four momenta of the decay products, though, to perform relevant checks to guarantee that the simulation is physically correct after each boost. These boosts will be discussed in the following section.

5.3 Boosting $\overline{\nu_\mu}$

After generating the four-momentum of $\overline{\nu_\mu}$ in both approaches, we need to boost the $\overline{\nu_\mu}$ from the rest system of the μ^+ to the system of Δ^+ moving in space, as created by the GZK process. We need three boosts to attain this. The first two boosts use the generated four-momenta of π^+ and μ^+. First, the $\overline{\nu_\mu}$ is boosted from the rest system of the μ^+ to the generated four-momentum of the of the μ^+. Then, the $\overline{\nu_\mu}$ is boosted from the rest system of the π^+ to the generated four-momentum of the of the π^+. The formula used to boost the four-momentum in these cases is:

$$\begin{aligned} p^{0\,\prime}_Y &= \frac{1}{m_X}\left(p^0_Y p^0_X + p^1_Y p^1_X + p^2_Y p^2_X + p^3_Y p^3_X\right) \\ \overrightarrow{p_Y}' &= \overrightarrow{p_Y} + \overrightarrow{p_X}\frac{p^{0\,\prime}_Y + p^0_Y}{p^0_X + m_X} \end{aligned} \tag{81}$$

In this case the particle denoted by Y refers to the decay product particle. Particle Y is boosted from the rest frame of the mother particle X to the moving frame of particle X, which is generated using the procedure of Section 5.1. In this simulation it is the generated four-momentum of $\overline{\nu_\mu}$ which is boosted. $\overline{\nu_\mu}$ thus fulfills the role of the general particle Y in (81) .

The last boost consists of taking the rest frame vector of Δ^+ over to it's four-momentum when travelling through space. The four-momentum of the Δ^+ is not generated using the method of Section 5.1. The derivation can be seen in

Appendix A. The rest frame vector $p^{\mu}_{\Delta^+}$ is taken over into $p^{\mu\prime}{}_{\Delta^+}$:

$$p^{\mu\prime}{}_{\Delta^+} = \begin{pmatrix} \sqrt{p_p^2 + m_{\Delta^+}^2} \\ 0 \\ 0 \\ p_p \end{pmatrix} \tag{82}$$

$$p_p = \frac{m_{\Delta^+}^2 + m_p^2}{4E_{\mathrm{CMB}}} \tag{83}$$

This is the third and last boost applied on the four-momentum of the $\overline{\nu_\mu}$.

5.4 Checks

To check that every substep of the simulation is compliant with the laws of physics, we verify that the on-shell condition and conservation of four-momentum hold. These conditions have been mentioned before, but are stated again below in the notation of this section, again with : $X \to Y + Z$:

$$p_X^0 = p_Y^0 + p_Z^0 \tag{84}$$

$$p_X^i = p_Y^i + p_Z^i \quad i = 1, 2, 3 \tag{85}$$

$$m^2 = (p^0)^2 - (\overrightarrow{p} \cdot \overrightarrow{p}) \tag{86}$$

The on-shell relation is written using the inner product notation, to emphasize the method used to perform this check in the algorithm. These checks hold for all steps when using a precision of fifty decimals.

5.5 Selecting Glashow Resonance Candidates

After generating the four-momenta of $\overline{\nu_\mu}$ and performing the neccesarry checks, the possible Glashow resonance candidates are selected. The first component of the four-momentum, $p^0_{\nu_\mu}$, denotes the energy. The following energy ranges are used:

$$6.0 \text{ PeV} < p^0_{\nu_\mu} < 6.6 \text{ PeV} \tag{87}$$

$$4.0 \text{ PeV} < p^0_{\nu_\mu} < 10 \text{ PeV} \tag{88}$$

The first range, of (87), corresponds to and energy range of 6.3 PeV $\pm\Delta E$, with $\Delta E = \frac{2\Gamma_{\mathrm{W}} E_{\mathrm{GR}}}{M_{\mathrm{W}}} = 0.3$ PeV.[12] $\Gamma_{\mathrm{W}} = 2.1$ GeV designates the full width at half maximum for the Glashow resonance peak of the crossection. The second range, of (88), corresponds to the energy range where the crossection of the Glashow resonance is larger than the non-resonant crossection, see also Figure 3. This resonance range is used in e.g. [28]. The number of GR candidates are then compared for both ranges.

6 Results

In this section, the results will be discussed for a simulation of 100,000 particles. The procedure of Section 5 is followed, this gives us the the energy distribution for a $\overline{\nu_\mu}$ that originates from a GZK reaction and the amount of Glashow candidates per 100,000 that follow from this distribution. Images can be found on the next pages. Other results of the simulation, including intermediate results of the boost and spatial distributions of the neutrino four-momenta, can be found in the appendix.

The energy spectrum of the $\overline{\nu_\mu}$ can be seen in Figure 7. In both the two-body and three-body decay simulation, the energy distribution ranges from about 10^{10} MeV to approximately $5 \cdot 10^{13}$ MeV. The energy spectrum of the neutrinos peaks around 10^{13} MeV $= 10^4$ PeV. This peak lies multiple orders of magnitude above the Glashow resonance energy of 6.3 PeV.

The number of Glashow candidates, selected according to Section 5.5, can be seen in Figures 8 and 9. The GR candidate histograms are the result of 100 simulations of 100,000 particles. In Figure 8, it can be seen that there are approximately 2-15 GR candidates out of 100,000 simulated particles for the range 6.0 PeV $< \ p^0_{\nu_\mu} < 6.6$ PeV. In Figure 9, the GR candidates for the energy range 4.0 PeV $< \ p^0_{\nu_\mu} < 10$ PeV are given, resulting in about 60-100 GR candidates per 100,000 simulated particles.

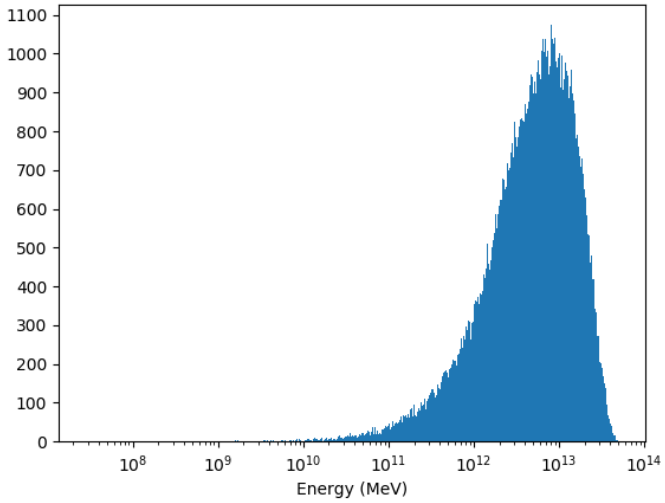

(a) Energy distribution generated in a two-body decay simulation.

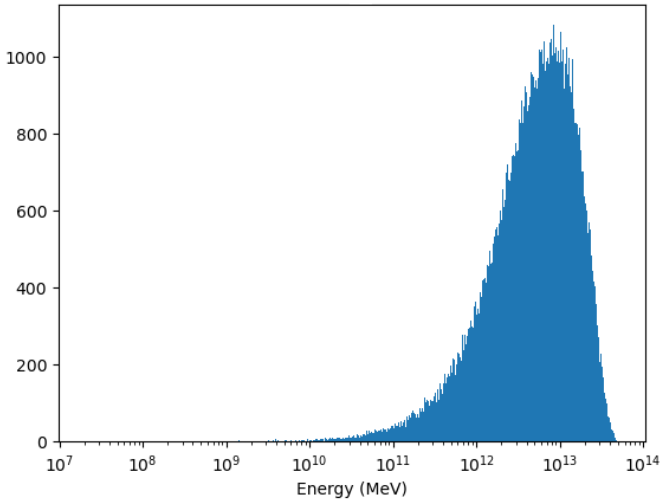

(b) Energy distribution generated in a three-body decay simulation

Figure 7: Histogram of the energy distribution of a GZK $\overline{\nu_\mu}$ in a simulation of 100,000 particles

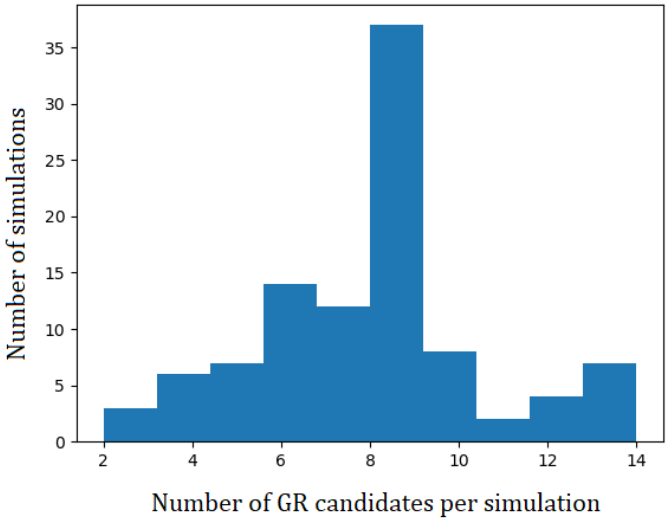

(a) Two-body decay simulation.

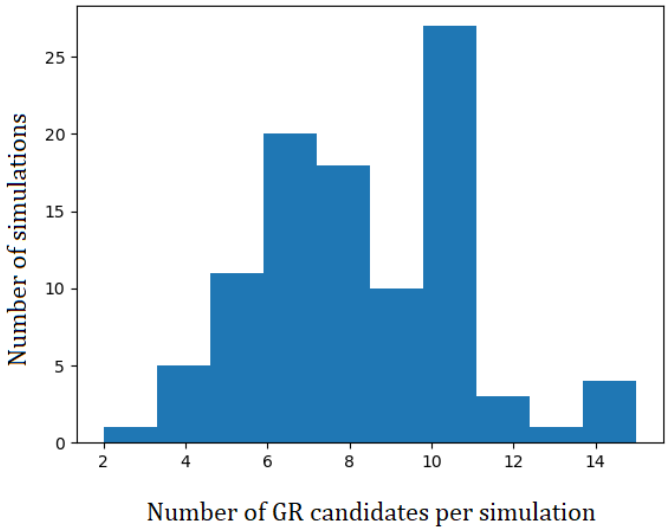

(b) Three-body decay simulation

Figure 8: Histogram of the number of $\overline{\nu_\mu}$ Glashow candidates for the energy range 6.0 PeV $< p^0_{\nu_\mu} <$ 6.6 PeV in a simulation of 100,000 particles.

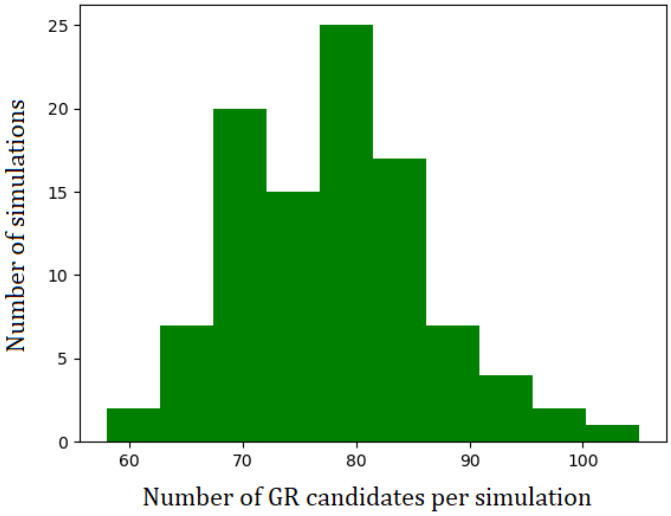

(a) Two-body decay simulation.

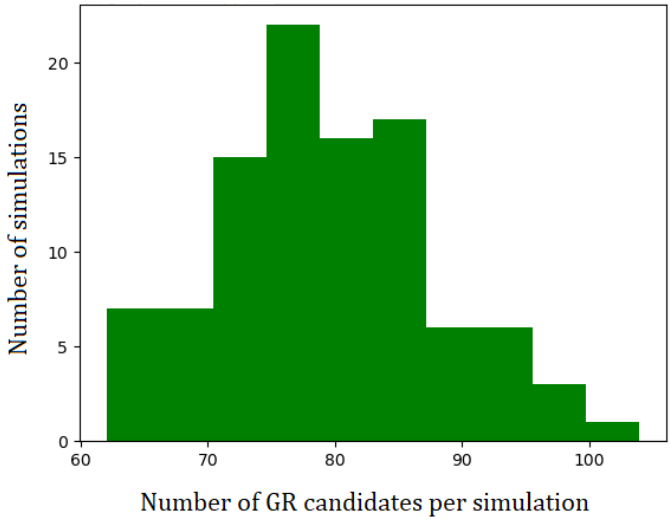

(b) Three-body decay simulation

Figure 9: Histogram of the number of $\overline{\nu_\mu}$ Glashow candidates for the energy range 4.0 PeV $< p^0_{\nu_\mu} <$ 10 PeV in a simulation of 100,000 particles.

7 Conclusion and Discussion

The conclusions we can draw from the results, as discussed above, are twofold. Firstly, one of the goals of the Monte Carlo simulation of the GZK process was to show that the two-body and three-body decay simulation would give the same results. This is logical, as both simulations describe the same physics. In Figure 7 we can indeed see that both simulations lead to the same energy spectrum for the $\overline{\nu_\mu}$. This in turn also gives similar results for the amount of GR candidates, as can be seen in Figures 8 and 9. Whereas the energy spectra of both simulation are approximately identical, the GR candidate histograms have some visible differences. This is probably not caused by a difference in the simulation, rather it is caused by the fact that random variables are used. As mentioned before, the GR candidate histograms are the result of 100 simulations of 100,000 particles. If we were to increase the number of simulations to a much higher amount, these histograms would very likely also become nearly indistinguishable. Unfortunately, this is not possible at the current moment, due to time constraints. To sum up, we can conclude that the two-body and three-body decay simulations give the same results, within the accuracy reached, as expected.

Secondly, we can conclude that the GZK process for pure proton UHECR could theoretically produce between 2 to 100 Glashow resonance candidates per 100,000 $\overline{\nu_\mu}$, depending on the energy range we choose. It is important to note that these candidates are muon neutrinos, not electron neutrinos. As discussed in Section 2.2, neutrino propagation through vacuum will lead to equal mixing of the flavour states. This assumption combined with the simulation shows us that there will be about 1-30 $\overline{\nu_e}$ that fall into the energy range relevant for Glashow resonance.

This is not a high amount, but it certainly is not negligible. Some remarks have to be made regarding this result. The first is the fact that we did not focus on the flux of these GZK neutrinos on Earth. A very low flux or a very high flux makes a large difference when talking about the experimental feasability of measuring GZK neutrinos using the Glashow resonance. Another note concerns the shape of the energy spectrum of the neutrinos. As seen in Figure 7, the main part of the peak lies above 10^{10} MeV. This energy is already about an order of magnitude above the Glashow resonance energy of 6.3 PeV = 6.3 $\cdot 10^9$ MeV. The GR candidates are almost invisible in the histogram of the energy spectrum. This leads to the question: are these GR candidates a legitimate outcome of the simulation or are they statistical outliers due to the use of random variables? And if the GR candidates would be statistical outliers, what implications would this have for the possibility of measuring GZK neutrinos using the Glashow resonance? Statistical outliers need not necessarily be unphysical, so this requires further research.

The result of the energy spectrum of the observation can also be qualitatively compared with some other results. For pure protons producing secondary

neutrinos, Kotera et al. and Aloiso et al. find similarly shaped energy spectra for the flux of cosmogenic neutrinos, although their results show a wider energy distribution, peaking around slightly lower energies.[31, 32] It is important to note that this is an informal qualitative comparison with the results stated above: Kotera et al. and Aloiso et al. express their results in neutrino flux, rather than bin counts, and Kotera et al. consider all neutrino flavours of the secondary GZK neutrinos.

Finally, we want to consider the current state of research on GZK neutrinos. As of this moment, UHE cosmogenic neutrinos have not been observed yet, but research is ongoing.[3, 33] There also have not been any Glashow resonance neutrinos observations at the moment.[20] Interestingly, there have been some observations of neutrinos in the PeV range, though not at 6.3 PeV. The observed PeV neutrinos are mainly in the 1-2 PeV range, which could point to a subdominant decay mode, but there is no reason why this would be preferred over the dominant hadronic decay mode. This could point to a 'missing Glashow resonance problem'.[22][5]

The lack of Glashow resonance events leads to constraints on the origins of cosmogenic neutrinos. The absence can for example be explained by a preference for $p\gamma$ (the GZK process) over pp interactions as the origin of cosmogenic neutrinos. In the case that no GR neutrinos are observed, this could imply that the muons lose energy before they decay, which inhibits their decay. [20, 22] This is the so called 'damped μ^+ mode'. A lack of GR events could also point towards a preference over $p\gamma$ over $A\gamma$ interactions. [12] The current observations could also imply constraints on the index of the neutrino energy spectrum.[12, 27, 30] Another possibility is that the cosmic rays with the highest energies are not protons but heavier nuclei.[10] In this case, a lower cosmogenic neutrino flux is expected.[36] This lower flux would imply there are less possible GR candidates. Finally, it is possible that the contribution of the Glashow resonance is not that significant, relative to other processes, when observing cosmogenic neutrinos.[14] In the future, observations of IceCube-Gen2 could make GR events more accessible, possibly giving increased GR neutrino data.[3] Even with the current lack of GR observations, there still is a large research interest in measuring GR neutrinos. As mentioned before, one of the advantages of GR events is that they are flavour specific: only $\overline{\nu_e}$ are sensitive to the resonance. This in turn makes Glashow resonance and interesting candidate to probe BSM physics, such as neutrino decay.[4, 25]

Finally, we can conclude the hunt for the Glashow resonance neutrinos is far from over. Large scale experiments such as GRAND and IceCube-Gen2 show us that the field of cosmogenic neutrino observation is booming. Time will tell what we can learn from these new neutrino measurements.

[5] Some papers mention that IceCube observed a GR neutrino. These results have been presented at conferences.[34, 35] I leave them out of consideration here, as these IceCube results have not been officially published yet.

Bibliography

[1] Luis A. Anchordoqui. "Ultra-high-energy cosmic rays". In: *Physics Reports* 801 (2019). Ultra-high-energy cosmic rays, pp. 1–93. ISSN: 0370-1573. DOI: https://doi.org/10.1016/j.physrep.2019.01.002. URL: http://www.sciencedirect.com/science/article/pii/S037015731930002X.

[2] Jaime Álvarez-Muñiz et al. "The Giant Radio Array for Neutrino Detection (GRAND): Science and design". In: *Science China Physics, Mechanics Astronomy* 63.1 (Aug. 2019). ISSN: 1869-1927. DOI: 10.1007/s11433-018-9385-7. URL: http://dx.doi.org/10.1007/s11433-018-9385-7.

[3] The IceCube-Gen2 Collaboration et al. *IceCube-Gen2: The Window to the Extreme Universe*. 2020. arXiv: 2008.04323 [astro-ph.HE].

[4] Markus Ackermann et al. *Fundamental Physics with High-Energy Cosmic Neutrinos*. 2019. arXiv: 1903.04333 [astro-ph.HE].

[5] Kenneth Greisen. "End to the Cosmic-Ray Spectrum?" In: *Phys. Rev. Lett.* 16 (17 Apr. 1966), pp. 748–750. DOI: 10.1103/PhysRevLett.16.748. URL: https://link.aps.org/doi/10.1103/PhysRevLett.16.748.

[6] G. T. Zatsepin and V. A. Kuz'min. "Upper Limit of the Spectrum of Cosmic Rays". In: *Soviet Journal of Experimental and Theoretical Physics Letters* 4 (Aug. 1966), p. 78.

[7] R U Abbasi et al. *Observation of the GZK Cutoff by the HiRes Experiment*. Tech. rep. astro-ph/0703099. RU-PNA-002. Comments: 4 pages, 4 figures, submitted to PRL. Mar. 2007. URL: https://cds.cern.ch/record/1021713.

[8] Markus Ahlers and Francis Halzen. "High-energy cosmic neutrino puzzle: a review". In: *Reports on Progress in Physics* 78.12 (Oct. 2015), p. 126901. DOI: 10.1088/0034-4885/78/12/126901. URL: https://doi.org/10.1088%5C%2F0034-4885%5C%2F78%5C%2F12%5C%2F126901.

[9] IceCube Collaboration et al. *Constraints on the Extremely-high Energy Cosmic Neutrino Flux with the IceCube 2008-2009 Data*. 2011. arXiv: 1103.4250 [astro-ph.CO].

[10] A. Aab et al. "Inferences on mass composition and tests of hadronic interactions from 0.3 to 100 EeV using the water-Cherenkov detectors of the Pierre Auger Observatory". In: *Phys. Rev. D* 96 (12 Dec. 2017), p. 122003. DOI: 10.1103/PhysRevD.96.122003. URL: https://link.aps.org/doi/10.1103/PhysRevD.96.122003.

[11] Guo-yuan Huang and Qinrui Liu. "Hunting the Glashow resonance with PeV neutrino telescopes". In: *Journal of Cosmology and Astroparticle Physics* 2020.03 (Mar. 2020), pp. 005–005. ISSN: 1475-7516. DOI: 10.1088/1475-7516/2020/03/005. URL: http://dx.doi.org/10.1088/1475-7516/2020/03/005.

[12] Daniel Biehl et al. "Astrophysical neutrino production diagnostics with the Glashow resonance". In: *Journal of Cosmology and Astroparticle Physics* 2017.01 (Jan. 2017), pp. 033–033. ISSN: 1475-7516. DOI: 10.1088/1475-7516/2017/01/033. URL: http://dx.doi.org/10.1088/1475-7516/2017/01/033.

[13] Markus Ahlers and Francis Halzen. "Opening a new window onto the universe with IceCube". In: *Progress in Particle and Nuclear Physics* 102 (2018), pp. 73–88. ISSN: 0146-6410. DOI: https://doi.org/10.1016/j.ppnp.2018.05.001. URL: http://www.sciencedirect.com/science/article/pii/S0146641018300346.

[14] Esteban Roulet et al. "PeV neutrinos from the propagation of ultra-high energy cosmic rays". In: 2013.1, 028 (Jan. 2013), p. 028. DOI: 10.1088/1475-7516/2013/01/028. arXiv: 1209.4033 [astro-ph.HE].

[15] Hans Niederhausen. *Recent IceCube Measurements Using High Energy Neutrinos*. 2019. arXiv: 1909.12182 [astro-ph.HE].

[16] A. Aab et al. "Probing the origin of ultra-high-energy cosmic rays with neutrinos in the EeV energy range using the Pierre Auger Observatory". In: *Journal of Cosmology and Astroparticle Physics* 2019.10 (Oct. 2019), pp. 022–022. DOI: 10.1088/1475-7516/2019/10/022. URL: https://doi.org/10.1088%5C%2F1475-7516%5C%2F2019%5C%2F10%5C%2F022.

[17] M. G. Aartsen et al. "Differential limit on the extremely-high-energy cosmic neutrino flux in the presence of astrophysical background from nine years of IceCube data". In: 98.6, 062003 (Sept. 2018), p. 062003. DOI: 10.1103/PhysRevD.98.062003.

[18] Ke Fang et al. *The Giant Radio Array for Neutrino Detection (GRAND): Present and Perspectives*. 2017. arXiv: 1708.05128 [astro-ph.IM].

[19] Sheldon L. Glashow. "Resonant Scattering of Antineutrinos". In: *Phys. Rev.* 118 (1 Apr. 1960), pp. 316–317. DOI: 10.1103/PhysRev.118.316. URL: https://link.aps.org/doi/10.1103/PhysRev.118.316.

[20] V. Barger et al. "Glashow resonance as a window into cosmic neutrino sources". In: *Physical Review D* 90.12 (Dec. 2014). ISSN: 1550-2368. DOI: 10.1103/physrevd.90.121301. URL: http://dx.doi.org/10.1103/PhysRevD.90.121301.

[21] Atri Bhattacharya et al. *On the interpretation of IceCube cascade events in terms of the Glashow resonance*. 2012. arXiv: 1209.2422 [hep-ph].

[22] Sarira Sahu and Bing Zhang. "On the non-detection of Glashow resonance in IceCube". In: *Journal of High Energy Astrophysics* 18 (2018), pp. 1–4. ISSN: 2214-4048. DOI: https://doi.org/10.1016/j.jheap.2018.01.003. URL: http://www.sciencedirect.com/science/article/pii/S221440481830003X.

[23] Atri Bhattacharya et al. "The Glashow resonance at IceCube: signatures, event rates andppvs.p interactions". In: *Journal of Cosmology and Astroparticle Physics* 2011.10 (Oct. 2011), pp. 017–017. ISSN: 1475-7516. DOI: 10.1088/1475-7516/2011/10/017. URL: http://dx.doi.org/10.1088/1475-7516/2011/10/017.

[24] J. A. Formaggio and G. P. Zeller. "From eV to EeV: Neutrino cross sections across energy scales". In: *Reviews of Modern Physics* 84.3 (Sept. 2012), pp. 1307–1341. ISSN: 1539-0756. DOI: 10.1103/revmodphys.84.1307. URL: http://dx.doi.org/10.1103/RevModPhys.84.1307.

[25] Ian M. Shoemaker and Kohta Murase. "Probing BSM neutrino physics with flavor and spectral distortions: Prospects for future high-energy neutrino telescopes". In: *Physical Review D* 93.8 (Apr. 2016). ISSN: 2470-0029. DOI: 10.1103/physrevd.93.085004. URL: http://dx.doi.org/10.1103/PhysRevD.93.085004.

[26] IceCube-Gen2 Collaboration et al. *IceCube-Gen2: A Vision for the Future of Neutrino Astronomy in Antarctica*. 2014. arXiv: 1412.5106 [astro-ph.HE].

[27] Andrea Palladino et al. "Double pulses and cascades above 2 PeV in IceCube". In: *The European Physical Journal C* 76.2 (Jan. 2016). ISSN: 1434-6052. DOI: 10.1140/epjc/s10052-016-3893-3. URL: http://dx.doi.org/10.1140/epjc/s10052-016-3893-3.

[28] Luis A. Anchordoqui et al. "Evidence for a break in the spectrum of astrophysical neutrinos". In: *Physical Review D* 95.8 (Apr. 2017). ISSN: 2470-0029. DOI: 10.1103/physrevd.95.083009. URL: http://dx.doi.org/10.1103/PhysRevD.95.083009.

[29] Matthew D. Kistler and Ranjan Laha. "Multi-PeV Signals from a New Astrophysical Neutrino Flux beyond the Glashow Resonance". In: *Physical Review Letters* 120.24 (June 2018). ISSN: 1079-7114. DOI: 10.1103/physrevlett.120.241105. URL: http://dx.doi.org/10.1103/PhysRevLett.120.241105.

[30] Sergio Palomares-Ruiz, Aaron C. Vincent, and Olga Mena. "Spectral analysis of the high-energy IceCube neutrinos". In: *Physical Review D* 91.10 (May 2015). ISSN: 1550-2368. DOI: 10.1103/physrevd.91.103008. URL: http://dx.doi.org/10.1103/PhysRevD.91.103008.

[31] Roberto Aloisio et al. "Cosmogenic neutrinos and ultra-high energy cosmic ray models". In: *Journal of Cosmology and Astroparticle Physics* 2015 (May 2015). DOI: 10.1088/1475-7516/2015/10/006.

[32] K Kotera, D Allard, and A.V Olinto. "Cosmogenic neutrinos: parameter space and detectabilty from PeV to ZeV". In: *Journal of Cosmology and Astroparticle Physics* 2010.10 (Oct. 2010), pp. 013–013. ISSN: 1475-7516. DOI: 10.1088/1475-7516/2010/10/013. URL: http://dx.doi.org/10.1088/1475-7516/2010/10/013.

[33] M. G. Aartsen et al. “Differential limit on the extremely-high-energy cosmic neutrino flux in the presence of astrophysical background from nine years of IceCube data”. In: *Physical Review D* 98.6 (Sept. 2018). ISSN: 2470-0029. DOI: 10.1103/physrevd.98.062003. URL: http://dx.doi.org/10.1103/PhysRevD.98.062003.

[34] Ignacio Taboada. “A View of the Universe with the IceCube and ANTARES Neutrino Telescopes”. In: *XXVIII International Conference on Neutrino Physics and Astrophysics*. June 2018, p. 35. DOI: 10.5281/zenodo.1286919.

[35] Christian Haack. “Detection of a Neutrino Event at the Glashow Resonance Energy in IceCube”. In: *The European Physical Society Conference on High Energy Physics 2019*. July 2019. URL: https://indico.cern.ch/event/577856/contributions/3422129/.

[36] Andrew M. Taylor, Markus Ahlers, and Dan Hooper. “Indications of negative evolution for the sources of the highest energy cosmic rays”. In: *Phys. Rev. D* 92 (6 Sept. 2015), p. 063011. DOI: 10.1103/PhysRevD.92.063011. URL: https://link.aps.org/doi/10.1103/PhysRevD.92.063011.

A Derivation of Δ^+ boost

In Section 5.3 the boost that takes the rest frame vector $p^{\mu}_{\Delta^+}$ over into the ${p^{\mu}}'_{\Delta^+}$ is written below.

$$p^{\mu}_{\Delta^+} = \begin{pmatrix} m^2_{\Delta^+} \\ 0 \\ 0 \\ 0 \end{pmatrix} \qquad {p^{\mu}}'_{\Delta^+} = \begin{pmatrix} \sqrt{p_p^2 + m^2_{\Delta^+}} \\ 0 \\ 0 \\ p_p \end{pmatrix}$$

A derivation of p_p is given here. A high energy proton, a cosmic ray, collides head on with a CMB photon. We set the direction of the momentum to the z-axis. This collision produces a Δ^+ at rest. The four-momenta for the proton and photon are:

$$p^{\mu}_{p} = \begin{pmatrix} E_p \\ 0 \\ 0 \\ p_p \end{pmatrix} \qquad p^{\mu}_{\gamma} = \begin{pmatrix} E_\gamma \\ 0 \\ 0 \\ -E_\gamma \end{pmatrix}$$

Using the fact that the proton has a very high energy, thus $E_p \gg m_p$, gives $E_p \approx p_p$. The derivation is then analogous to the derivation of the GZK limit energy, as seen in Section 2:

$$\begin{aligned} m^2_{\Delta^+} &= \left(p^{\mu}_{p} + p^{\mu}_{\gamma}\right)^2 \\ m^2_{\Delta^+} &= p_p \cdot p_p + p_\gamma \cdot p_\gamma + 2p_\gamma \cdot p_p \\ m^2_{\Delta^+} &= m_p^2 + 0 + 2(E_p E_\gamma - (-p_p E_\gamma)) \\ m^2_{\Delta^+} &\overset{E_p \approx p_p}{=} m_p^2 + 4p_p E_\gamma \\ p_p &= \frac{m^2_{\Delta^+} - m_p^2}{4E_\gamma} \end{aligned}$$

B Additional Results

B.1 Two-body Decay Monte Carlo Simulation of $\overline{\nu_\mu}$

In this section, all results of the simulation of the four-momentum of the $\overline{\nu}_\mu$ are given for a two-body decay simulation, including all intermediate results of the Lorentz boost. All simulations consider 100,000 particles. The images show that the spatial part of the four-momentum is isotropic, as expected, for all (boosted) four-momenta except for the last boost. This is due to the fact that the for last boost we constrained the spatial boost to the z-axis. In this simulation, the neutrino is a product of the decay $\mu^+ \to \overline{\nu_\mu} + W^+$, where W^+ has a variable mass.

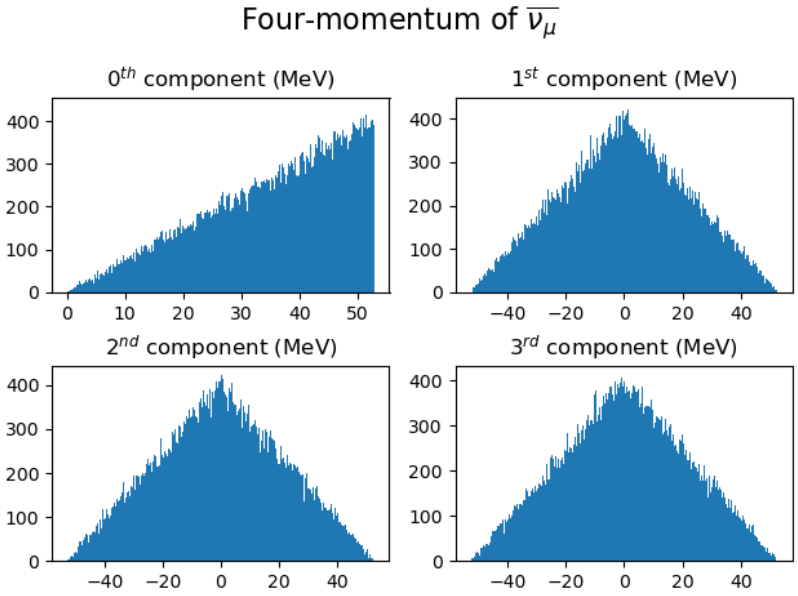

Figure 10: Simulation of four-momentum of $\overline{\nu_\mu}$ in the restsystem of the muon for two-body decay.

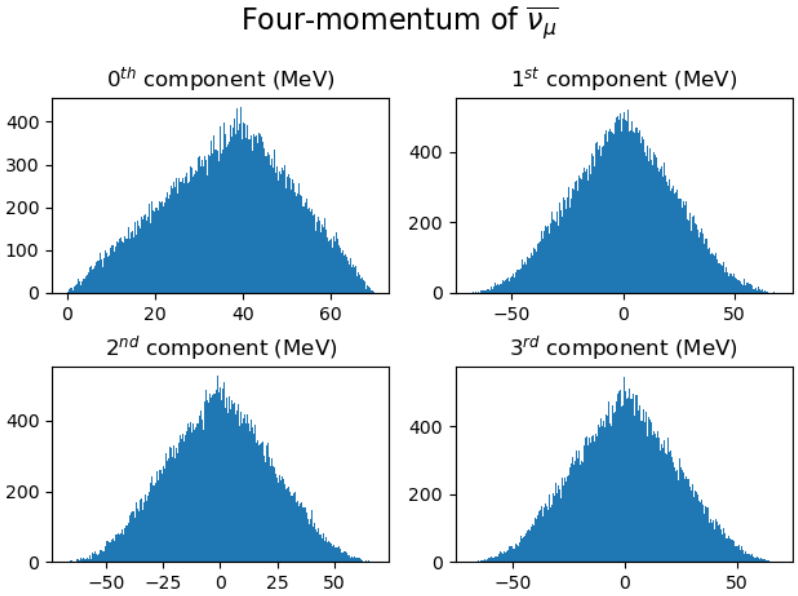

Figure 11: Simulation of four-momentum of $\overline{\nu_\mu}$ in the restsystem of the pion for two-body decay.

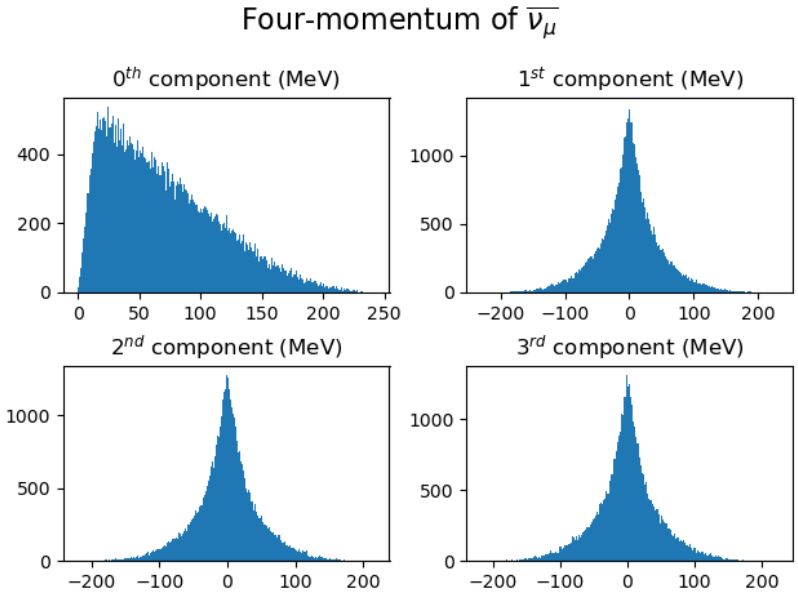

Figure 12: Simulation of four-momentum of $\overline{\nu_\mu}$ in the restsystem of the Δ^+ for two-body decay.

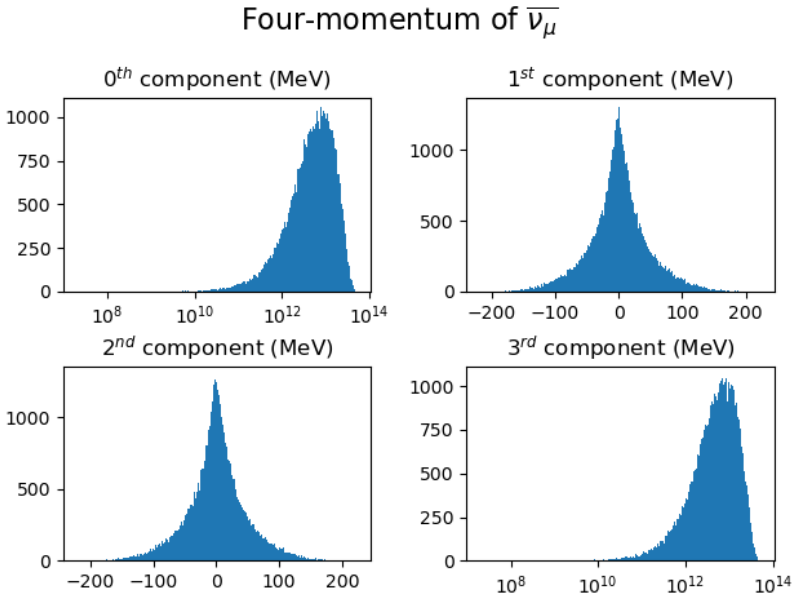

Figure 13: Simulation of four-momentum of $\overline{\nu_\mu}$ in the boosted system of the Δ^+ for two-body decay.

B.2 Three-body Decay Monte Carlo Simulation of $\overline{\nu_\mu}$

In this section, all results of the simulation of the four-momentum of the $\overline{\nu}_\mu$ are given for a three-body decay simulation, including all intermediate results of the Lorentz boost. All simulations consider 100,000 particles. The images show that the spatial part of the four-momentum is isotropic, as expected, for all (boosted) four-momenta except for the last boost. This is due to the fact that the for last boost we constrained the spatial boost to the z-axis. In this simulation, the neutrino is a product of the decay $\mu^+ \to \overline{\nu_\mu} + e^+ + \nu_e$.

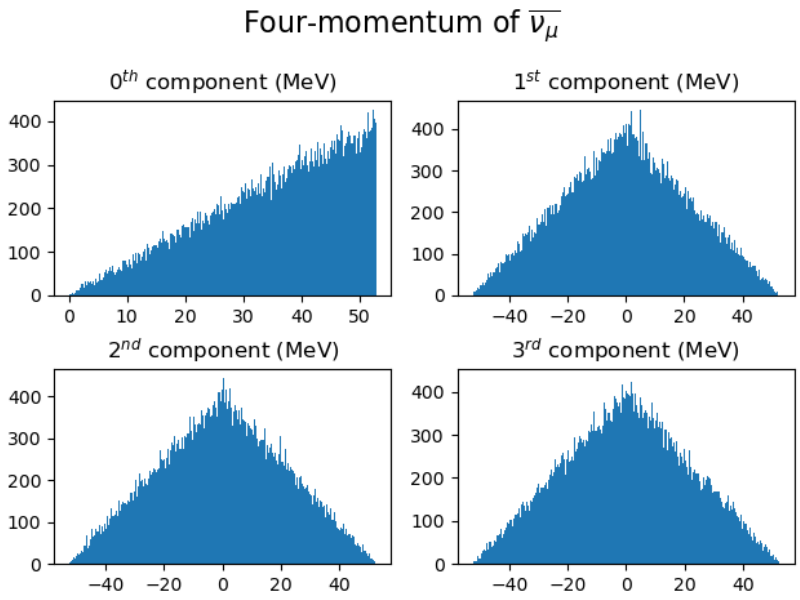

Figure 14: Simulation of four-momentum of $\overline{\nu_\mu}$ in the restsystem of the muon for three-body decay.

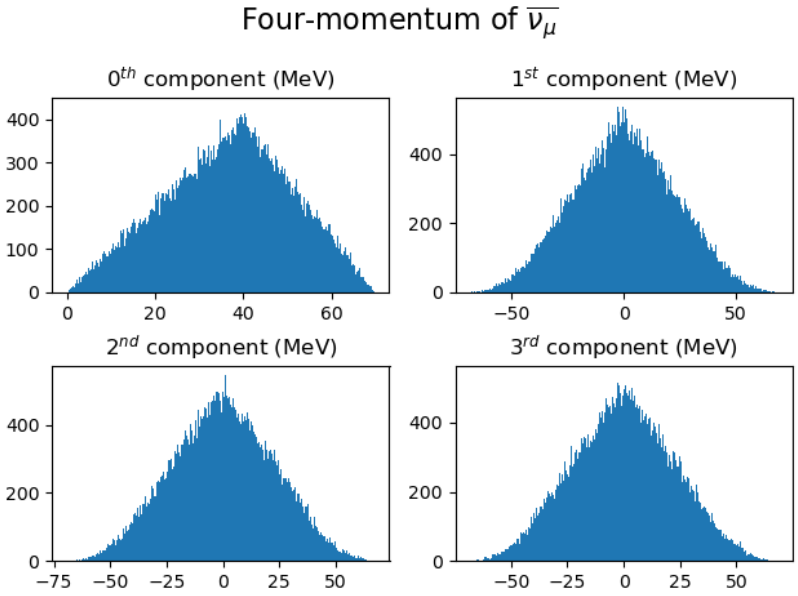

Figure 15: Simulation of four-momentum of $\overline{\nu_\mu}$ in the restsystem of the pion for three-body decay.

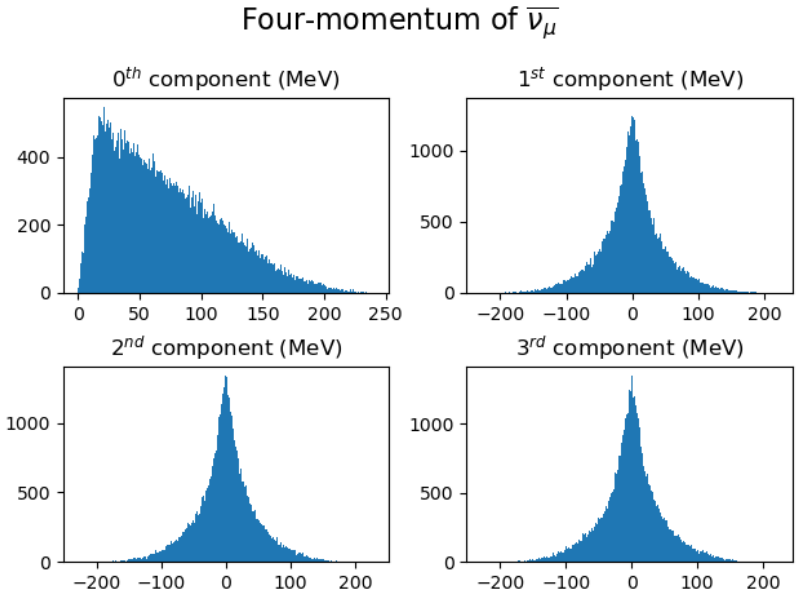

Figure 16: Simulation of four-momentum of $\overline{\nu_\mu}$ in the restsystem of the Δ^+ for three-body decay.

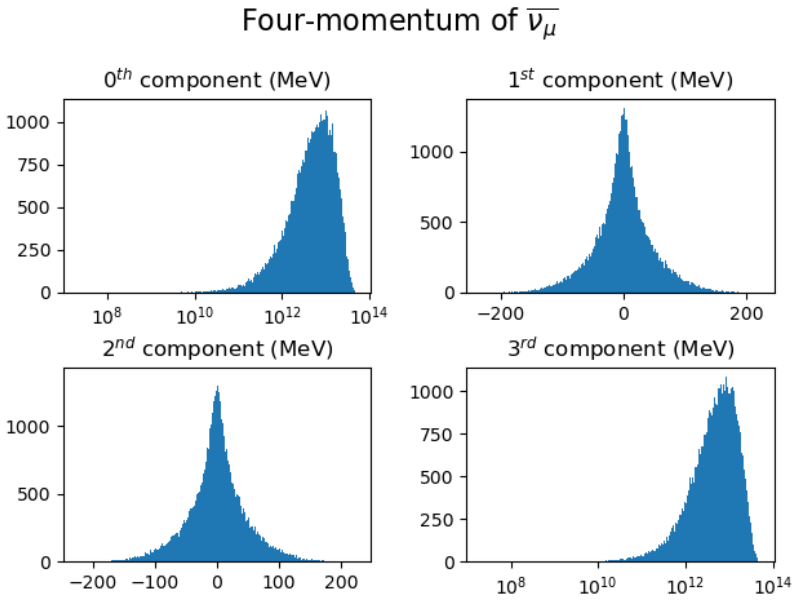

Figure 17: Simulation of four-momentum of $\overline{\nu_\mu}$ in the boosted system of the Δ^+ for three-body decay.

B.3 Generated Mass of W-boson

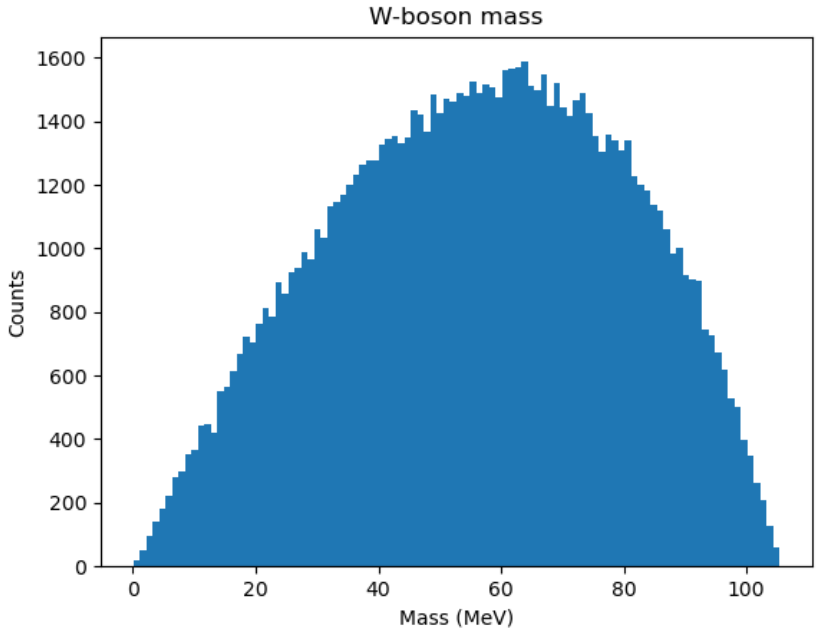

Figure 18: The generated masses of the W-boson according to the distribution given in Section 5.2.1